Irradiation-induced phase transformations in zirconium alloys

L. M. Howe[a], D. Phillips[a], A. T. Motta[b] and P. R. Okamoto[c]

[a]*Reactor Materials Research Branch, AECLResearch, Chalk River Laboratories, Chalk River, Ont. KOJ 1JO (Canada)*

[b]*Department of Nuclear Engineering, The Pennsylvania State University, University Park, PA 16802 (USA)*

[c]*Materials Science Division, Argonne National Laboratory, Argonne, IL 60439 (USA)*

Abstract

Ion and electron irradiations were used to follow the irradiation-induced crystalline-to-amorphous transformation in Zr_3Fe, $ZrFe_2$, $Zr(Cr,Fe)_2$ and $ZrCr_2$, as well as in $Zr(Cr,Fe)_2$ and $Zr_2(Ni,Fe)$ precipitates in Zircaloy-4. [40]Ar and [209]Bi ion irradiations of Zr_3Fe were performed at 35–725 K using ions of energy 15–1500 keV. The effect of the deposited-energy density $\bar{\theta}_v$ in the collision cascade on the nature of the damaged regions in individual cascades was investigated. The amorphization kinetics of Zr_3Fe during *in situ* electron irradiation were also determined. The electron fluence required for amorphization increased exponentially with temperature, and the critical temperature for amorphization was about 220 K, compared with 575–625 K for ion irradiation. The difference between the heavy ion and electron irradiation results is attributed to the fact that ion irradiation produces displacement cascades, while electron irradiation produces isolated Frenkel pairs. The dependence of the damage production on the incident electron energy was determined for Zr_3Fe and the results could be analysed in terms of a composite displacement cross-section dominated at high energies by displacements of Zr and Fe atoms; by displacements of Fe atoms at intermediate energies; and by secondary displacements of lattice atoms by recoil impurities at low energies. An investigation was initiated on $ZrFe_2$, $Zr(Cr,Fe)_2$ and $ZrCr_2$ to study the effect of variation of the stoichiometry and the presence of lattice defects on irradiation-induced amorphization. The irradiation-induced amorphization of the intermetallic precipitates $Zr(Cr,Fe)_2$ and $Zr_2(Ni,Fe)$ in Zircaloy-4 was also studied during *in situ* bombardment by [40]Ar ions of energy 350 keV. The amorphization morphology was shown to be homogeneous. These results are discussed in the context of previous experimental results of neutron and electron irradiations, and likely amorphization mechanisms are proposed.

1. Introduction

The irradiation behavior of the various intermetallic compounds of Zr-containing Fe, Cr, Ni, Sn and Si, which are found in the fuel cladding and pressure tubes (such as Zircaloy-2, Zircaloy-4 and Zr–2.5Nb alloys) in water-cooled nuclear reactors, is of technological interest. An irradiation-induced crystalline-to-amorphous transformation has been observed for $Zr(Cr,Fe)_2$ and $Zr_2(Ni,Fe)$ precipitates in Zircaloy-2 and Zircaloy-4 (see, for example, refs. 1–4). Depending upon the precipitate, temperature of irradiation and nature of the bombarding projectile, the transformation could occur with or without a concurrent preferential depletion of Fe from the precipitates. The intermetallic compounds Zr_3Fe [5–8], Zr_2Ni [9, 10], $ZrNi$ [10] and $ZrNi_3$ [10] also can be rendered amorphous by irradiation. Irradiation-induced redistribution of Fe also has been observed in neutron-irradiated Zr alloys [2, 11, 12], and is associated with accelerated irradiation growth. Consequently, it is of considerable interest to obtain more detailed information on the mass transport of Fe in irradiated Zr alloys, including the irradiation behavior of various intermetallic compounds (Zr_3Fe, Zr_2Fe, $ZrFe_2$, $ZrCr_2$, $Zr(Cr,Fe)_2$ and $Zr_2(Ni,Fe)$).

In this investigation, results are presented on the effect of the deposited-energy density $\bar{\theta}_v$ on the nature of the damaged regions in individual cascades produced by ion bombardment of Zr_3Fe. A detailed comparison is also made between irradiation-induced amorphization of Zr_3Fe during electron irradiation [8] and that under ion bombardment [5–7]. The dependence of the damage production on the incident electron energy in Zr_3Fe also has been determined. Preliminary results are also discussed for the amorphization of $ZrFe_2$, $Zr(Cr,Fe)_2$ and $ZrCr_2$ by electron irradiation. The results of a recent investigation [13] on the amorphization of $Zr(Cr,Fe)_2$ and $Zr_2(Ni,Fe)$ precipitates are discussed in the context of previous experimental results of neutron and electron irradiations, and likely amorphization mechanisms are proposed.

2. Experimental details

The Zr_3Fe and $ZrFe_2$ materials used in the investigation were obtained by prolonged heat treatment of Zr–Fe alloys containing 20.0, 25.0 and 75.0 at.% Fe, which had been prepared by arc melting. $ZrCr_2$ and $Zr(Cr,Fe)_2$ were made in a similar fashion. The irradiation behavior of $Zr(Cr,Fe)_2$ and $Zr_2(Ni,Fe)$ precipitates in Zircaloy-4 was also investigated. Zr_3Fe has an ortho-

rhombic crystal structure, while $ZrFe_2$, $Zr(Fe,Cr)_2$ and $ZrCr_2$ have the $MgZn_2$ Laves phase structure, and $Zr_2(Ni,Fe)$ has the C16 body-centered tetragonal (b.c.t.) structure. Discs 0.30 cm in diameter were produced from all the above alloys by a combination of spark cutting, spark planing, mechanical polishing and electropolishing operations.

The samples were irradiated at 35–725 K with ^{40}Ar or ^{209}Bi ions in either the Chalk River high-voltage mass separator or the Chalk River 70 kV isotope separator. They were surrounded by a cryoshield operating at about 20 K, which maintained ultrahigh vacuum (UHV) conditions around the target during the ion implant- ation. For studies of the nature of the damage produced in individual cascades (or early stages of cascade over- lap), monoenergetic (15–350 keV) ^{209}Bi ion implants were performed at 35–40 K to fluences of $1.0–7.5 \times 10^{11}$ ion cm^{-2}. Investigations of the irradia- tion-induced crystalline-to-amorphous transformation were performed at 35–725 K using successively ^{40}Ar or ^{209}Bi ions of energy 1.5, 1.0 and 0.5 MeV. Weighted ion fluences were used for the three different energies of the ion beams. The irradiation damage produced during the ion bombardments was distributed over depths of about 1 and 0.3 μm for the ^{40}Ar and ^{209}Bi ions respectively.

Transmission electron microscopy (TEM) examina- tions were performed at 295 K in a Philips CM30 electron microscope operating at 300 kV. Analytical electron microscopy (AEM) was also performed from selected areas of the irradiated specimens, using the CM30 coupled to a Link X-ray analysing system.

To obtain kinetic information on the irradiation- induced amorphization of the intermetallic compounds, *in situ* irradiations and observations were made using the dual-ion-beam high-voltage electron microscope (HVEM) facility at Argonne National Laboratory (ANL). The irradiations were performed at 23–650 K using either electrons of energy 200–900 keV or ^{40}Ar ions of energy 350 keV.

3. Results and discussion

3.1. Collision Cascades in Zr_3Fe

It will be useful to discuss the experimental results in terms of the average deposited-energy density $\bar{\theta}_v$ in the cascade [14–18]. $\bar{\theta}_v$ is a measure of the average amount of energy expended in nuclear collision events, which is deposited per atom in the volume occupied by an individual collision cascade.

For monatomic ion implants, $\bar{\theta}_v$ will be defined as [14–18]

$$\bar{\theta}_v = 0.2 v(E)/N_V V_R \tag{1}$$

where $v(E)$ is the portion of the monatomic ion energy

that is lost in nuclear collision events, N_v is the number of lattice atoms contained within a spheroid whose axes are determined by the longitudinal $\langle \Delta X^2 \rangle^{1/2}$ and transverse $\langle Y^2 \rangle^{1/2}$ straggling components of the statisti- cal damage distribution [19, 20], and V_R is the volume ratio defining the fraction of the statistical volume filled on average by an individual cascade. Only about 20% of the total $v(E)$ will be contained within the statistical volume, so giving the factor 0.2 in eqn. (1).

$v(E)$, $\langle \Delta X^2 \rangle^{1/2}$, $\langle Y^2 \rangle^{1/2}$ and N_v were determined using the analytical theory outlined in refs. 19 and 20. Based upon Monte Carlo damage simulations, Walker and Thompson [14] determined that $V_R = 0.52$ for ^{209}Bi ions in Ge. The atomic charge Z and atomic weight A of Ge are 32 and 72.60, respectively, compared with the average values of Z and A for Zr_3Fe of 36.50 and 82.37. Hence, a value for V_R of 0.52 will also be used for ^{209}Bi ions in Zr_3Fe. For ^{209}Bi ion implants of energy 15, 30, 45, 60, 90, 120, 250, 350, 500, 1000 and 1500 keV in Zr_3Fe, the corresponding $\bar{\theta}_v$ values are 4.04, 1.96, 1.29, 0.94, 0.60, 0.42, 0.17, 0.11, 0.07, 0.03 and 0.01 eV at^{-1}.

Using various operating reflections, the damaged regions produced by ^{209}Bi ion bombardment of Zr_3Fe were imaged under dynamical conditions in the electron microscope, as shown in Figs. 1(a) and 1(b). Detailed bright and dark-field analysis indicated that the damaged regions were not dislocation loops, stacking fault tetrahe- dra or either vacancy or interstitial clusters having an appreciable strain field. Instead, they appeared to be regions in the crystal exhibiting strong structure factor contrast and, consequently, probably have a significantly different structure from the crystalline matrix. This would be consistent with the damaged regions being essentially amorphous, as also indicated by TEM investi- gations on ion-bombarded Si, [15–18, 21–24], Ge [17, 25, 26] and $NiAl_3$ [27]. Damaged regions having similar features have also been seen in Zr_3Fe bombarded with ^{40}Ar ions of energy 0.5–1.5 MeV [6], including *in situ* bombardments and observations using ^{40}Ar ions of energy 350 keV [28].

At high deposited-energy densities ($\bar{\theta}_v > 2.0$ eV at^{-1}), which corresponds to fairly low Bi ion energies (15–30 keV), the visible damage produced in a single cascade consisted essentially of a single, isolated dam- aged region (Fig. 1(a)). With decreasing values of $\bar{\theta}_v$ (*i.e.* increasing ion implant energies), there was an increasing tendency for multiple damaged regions to form within a main cascade (Fig. 1(b)). The average values of the diameter of the damaged regions present in the electron micrographs were obtained and these were correlated with a particular cascade, as determined from the longitudinal $\langle \Delta X^2 \rangle^{1/2}$ and transverse $\langle Y^2 \rangle^{1/2}$ straggling components of the statistical volume. The initial results were given in ref. 7 and even more detailed measure- ments have now been performed. These measurements
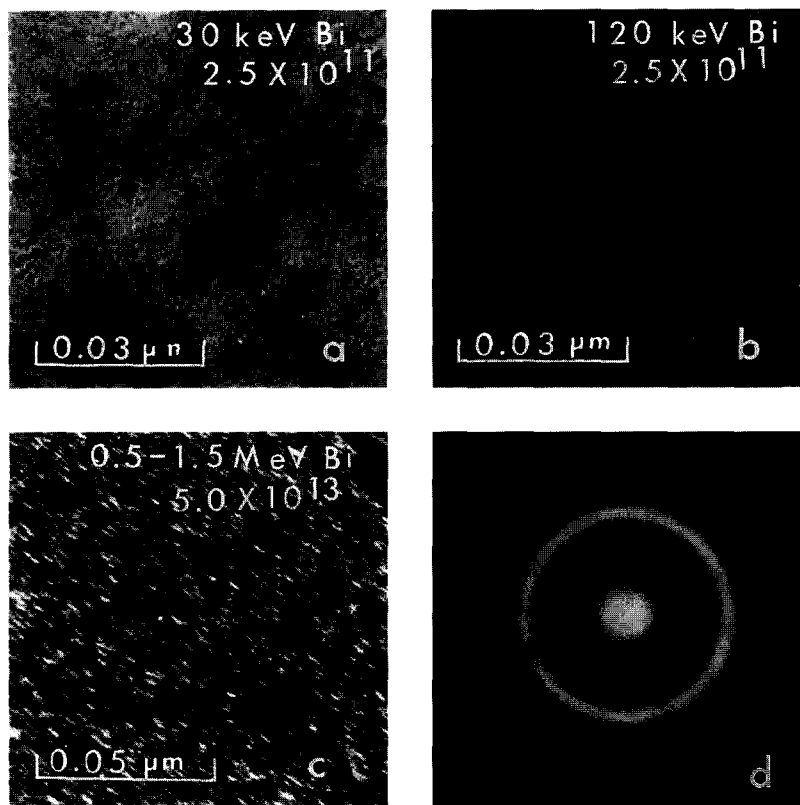
Fig. 1. (a)–(c) Bright-field electron micrographs and (d) diffraction pattern for Zr_3Fe bombarded with [209]Bi ions at the following energies and ion fluences: (a) 30 keV, 2.5×10^{11} ion cm^{-2}; (b) 120 keV, 2.5×10^{11} ion cm^{-2}; (c) 0.5–1.5 MeV, 5.0×10^{13} ion cm^{-2}; (d) 0.5–1.5 MeV, 5.0×10^{13} ion cm^{-2}.

were performed on Zr_3Fe bombarded with [209]Bi ions of energy 15–350 keV at fairly low ion fluences $(1.0$–2.5×10^{11} ion cm$^{-2})$ to avoid appreciable cascade overlap.

The number of multiple damaged regions (subcascades) formed within an individual collision cascade and the average total volume occupied by the subcascades within a cascade were determined from the detailed measurements performed on the visible damaged regions. As shown in Fig. 2, the average number n_{sc} of multiple damaged regions increased steadily from 1.1 at 15 keV to 3.1 at 350 keV. This is in good agreement with the results obtained for Si [18] and Ge [17] bombarded with various ions. Also shown in Fig. 2 is the fraction F of the theoretical volume (determined from the analytical theory outlined in refs. 19 and 20, as discussed previously) that was occupied on average by the visible multiple damaged regions comprising a cascade. The results show that F decreases quite rapidly with increasing ion energy (decreasing $\bar{\theta}_v$ values). Similar behavior was found in ion-implanted Ge and Si [17, 18]. The Ge [17] results are also plotted in Fig. 2 for comparison with the Zr_3Fe results. For [209]Bi ion implants of energy 10, 15, 30, 45, 60, 90 and 120 keV implants in Ge, the corresponding $\bar{\theta}_v$ values are 4.10, 2.75, 1.28, 0.83, 0.61, 0.38 and 0.27 eV at^{-1}.

The above results for Zr_3Fe, as well as those for Si and Ge [17, 18], emphasize the important distinction between very high deposited-energy density cascades $(\bar{\theta}_v > 2$ eV at$^{-1})$ and those of considerably lower deposited-energy density $(\bar{\theta}_v < 0.5$ eV at$^{-1})$. In the case of very high deposited-energy density cascades, appreciable fractions of the theoretical collision cascade volume (as defined above) have been rendered amorphous. This behavior is certainly consistent with the operation of an energy spike [15–18] for high deposited-energy density cascades, because this would explain why amorphous regions could extend over the whole of the theoretical collision cascade volume and even beyond it. In Ge, for example, $F = 0.93$ and 1.18 for Bi ion energies of 15 keV $(\bar{\theta}_v = 2.75$ eV at$^{-1})$ and 10 keV $(\bar{\theta}_v = 4.10$ eV at$^{-1})$ respectively [17] (see Fig. 2). In the lower deposited-energy density cascades, there are localized regions (i.e. subcascades) that are essentially amorphous, but these are obviously surrounded by areas (which are still within the single main cascade) having a high density of point defects and small defect clusters.

3.2. Irradiation-induced crystalline-to-amorphous transformation in Zr_3Fe

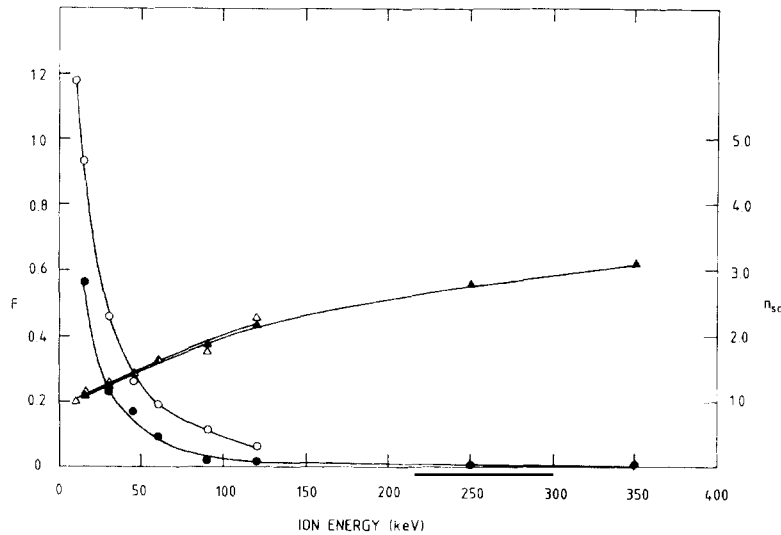Investigations have revealed that Zr_3Fe can be completely amorphized during irradiation with ^{40}Ar and

Fig. 2. Collision cascade parameters F (●, ○) and n_{sc} (▲, △) as a function of incident ion energy for ^{209}Bi ion irradiations of Zr_3Fe (full symbols) and Ge (Open symbols).

^{209}Bi ions [5–7], and electrons [8]. An example of this behavior is shown in Figs. 1(c) and 1(d) for ^{209}Bi ion bombardments. The criteria used to determine that an amorphous phase had been formed were the interruption of all the bend contours in the TEM images of the irradiated areas, and the disappearance of all crystalline spots from the diffraction patterns. A detailed study of the temperature dependence of the dose-to-amorphization has now been completed for irradiations with Ar ions of energy 0.5–1.5 MeV and the results are shown in Fig. 3.

It can be seen that, in the region 160–220 K, there is a step in the dose-to-amorphization curve, followed by a plateau region extending up to about 450 K. Preliminary results indicate that the magnitude of this step is less for irradiations with ^{209}Bi ions of energy 0.5–1.5 MeV than for similar ^{40}Ar ion irradiations. This would suggest that the magnitude decreases with increasing $\bar{\theta}_v$ values, which is consistent with the details of the damaged regions depending upon $\bar{\theta}_v$, as discussed above.

In the temperature range 160–280 K, there was a pronounced dose rate (flux) effect [6]. The fraction of the irradiated volume that had been rendered amorphous at a given ion fluence increased noticeably as the ion flux was increased from 0.9×10^{11} to 14.7×10^{11} ion cm^{-2} s^{-1}. For example, irradiation of Zr_3Fe at 180 K with ^{40}Ar ions (1.5, 1.0 and 0.5 MeV) to the same total ion fluence of 1.0×10^{15} ion cm^{-2} resulted in the production of amorphous regions throughout a heavily damaged crystalline matrix at an ion flux of 0.9×10^{11} ion cm^{-2} s^{-1}; strained crystalline regions in an amorphous matrix at an ion flux of 2.9×10^{11} ion cm^{-2} s^{-1}; and complete amorphization at an ion flux of 14.7×10^{11} ion cm^{-2} s^{-1}.
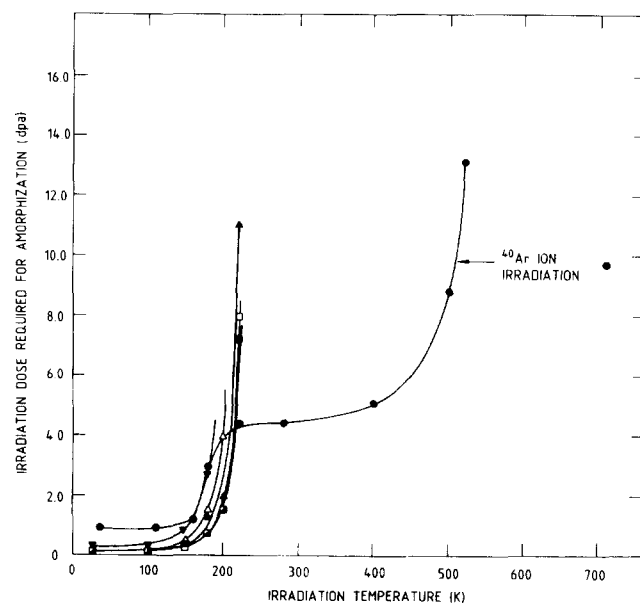

Fig. 3. Dose-to-amorphization, in displacements per atom (dpa), at various irradiation temperatures for 0.9 MeV electron and 0.5–1.5 MeV ^{40}Ar ion (●) irradiations of Zr_3Fe. Electron dose rate: ■, 1.83×10^{-3} dpa s^{-1}; □, 1.68×10^{-3} dpa s^{-1}; ▲, 1.47×10^{-3} dpa s^{-1}; △, 1.23×10^{-3} dpa s^{-1}; ▼, 1.04×10^{-3} dpa s^{-1}.

As shown in Fig. 3, the critical temperature for the amorphization of Zr_3Fe by ^{40}Ar ion irradiation was 570–600 K (i.e. Zr_3Fe could not be rendered amorphous during irradiation above this temperature), and preliminary investigations indicate that it is slightly higher (about 625 K) for ^{209}Bi ion irradiation. A critical temperature for amorphization (i.e. the temperature above which amorphization can no longer be achieved) of 570–625 K for the ion irradiations is consistent with the

observation that the discrete damaged regions produced during [40]Ar ion irradiations anneal out at about 400–500 K [6]. Also, in Zr_3Fe rendered completely amorphous during ion bombardment, small crystals were observed to form in the amorphous matrix during annealing for 0.5 h at 500–600 K, and extensive growth of crystalline regions was observed during annealing for 3 h at 623 K [5]. Neither the irradiation-induced crystalline-to-amorphous transformation nor its reversal during post-irradiation annealing produced any change in the chemical composition of the matrix, *i.e.* it remained as Zr_3Fe [5].

Irradiations of Zr_3Fe with electrons of energy 0.9 MeV were performed at 28–220 K in the HVEM at ANL. By measuring the onset, spread and final size of the amorphous region, as well as factoring in the gaussian distribution of the beam, a kinetic description of amorphization in terms of dose, dose rate and temperature was obtained [8]. The dose required to reach a given radius of the amorphous region (*i.e.* the dose-to-amorphization for a given dose rate) is shown as a function of the irradiation temperature in Fig. 3. The critical temperature for amorphization by electron irradiation was about 220 K, compared with 570–600 K for [40]Ar ion irradiation, as shown in Fig. 3. The dose-to-amorphization increased exponentially with temperature. Results also indicated that the rate of growth of the amorphous region under the electron beam decreased with increasing temperature, and the dose-to-amorphization decreased with increasing dose rate.

The results of the ion and electron irradiations can be understood in the framework of damage accumulation under irradiation. Damage produced by irradiation is opposed by thermal annealing. The balance between the rate of damage production and the ability of the material to repair itself dictates the response of the material to irradiation. At low temperatures, damage produced by irradiation remains "frozen in", with little annealing taking place. In this temperature regime, the dose-to-amorphization is almost independent of the temperature: the damage accumulates in the lattice, unchecked by thermal annealing. At a certain level of irradiation damage in Zr_3Fe, there appears to be a driving force to exchange the imperfect form of long-range order resulting from irradiation for a local configuration of short-range order, where the bonding restrictions of chemical species and directionality are followed more closely. The difference between the ion and electron irradiations results from the fact that ion irradiation produces displacement cascades, while electron irradiation produces isolated Frenkel pairs. Within the cascades, the density of damage is quite high and amorphization can then occur either directly in the cascade or upon cascade overlap. As the irradiation temperature increases, annealing processes are activated that offset the production of

damage. When annealing reduces the effective damage rate without overwhelming it, a "step" appears in the dose-to-amorphization *vs.* temperature curve, increasing the dose-to-amorphization at that temperature. The temperature at which the activated annealing process completely overwhelms damage production is the critical temperature, and amorphization is no longer possible above that temperature. It follows then that a lower damage rate is offset at a lower temperature than is a higher damage rate. This implies different critical temperatures for different damage rates.

The increase in dose-to-amorphization between 150 and 200 K under electron irradiation corresponds closely to the change in amorphization regime occurring between 110 and 160 K under [40]Ar ion irradiation. At 110 K and below, the dose-to-amorphization during [40]Ar ion irradiation is smaller than at 160 K. Below 160 K, the regions between cascades do not become annealed before the next cascade hits. At 160 K and above, some type of defect becomes mobile. The resulting defect annihilation produces a less damaged outer region of the cascade, leaving a smaller, heavily damaged core, thus requiring more extensive coverage of the material for complete amorphization.

Above about 400 K, different defects become mobile in Zr_3Fe than in the range 160–220 K. Eventually, sufficient annealing occurs in the damage cascades so that amorphization can no longer occur, even under ion irradiations. For [40]Ar ion irradiation of Zr_3Fe, this stage is reached at 570–600 K and, for [209]Bi ion irradiations of Zr_3Fe, the temperature is slightly higher (about 625 K). From investigations of amorphization in CuTi, Koike *et al.* [29] also concluded that, for similar fluxes (dose rates) of bombarding projectiles, the critical temperature for amorphization increased with the mass of the incident projectile (*i.e.* with increasing average deposited-energy density in the collision cascade).

A study was also undertaken to determine the energy dependence of the dose-to-amorphization during electron irradiation of Zr_3Fe at 23–30 K. Zr_3Fe samples were irradiated in the HVEM at ANL at energies from 200 to 900 keV. Amorphization occurred at energies from 900 down to 250 keV. Three distinct regions were observed, as shown in Fig. 4. Between 900 and 700 keV, amorphization occurred at a constant low dose of 5×10^{21} e$^-$ cm^{-2}; a higher plateau at 10^{22} e$^-$ cm^{-2} was observed between 600 and 400 keV; finally, there was a sharp increase in the dose-to-amorphization below 400 keV. At 250 keV, the dose required to amorphize Zr_3Fe was an order of magnitude higher than that at 900 keV.

A dependence of the dose-to-amorphization on the orientation of the sample relative to the electron beam was observed at low electron energies. This is apparent in Fig. 5(a), where the beam was centered on a triple
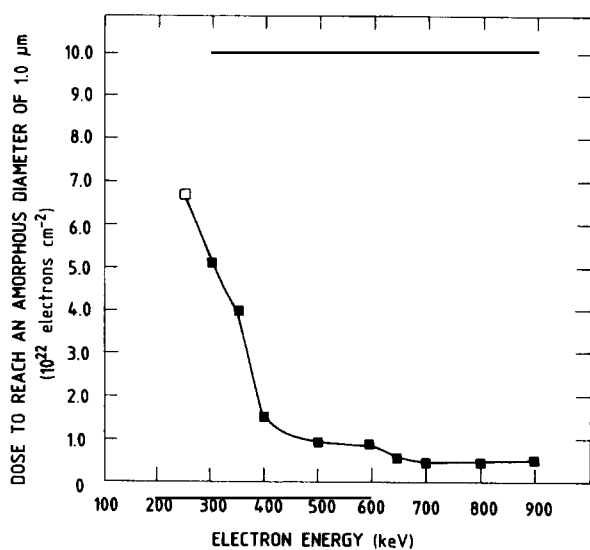
Fig. 4. Dose-to-amorphization for Zr_3Fe at 23–30 K as a function of the incident electron energy: □, restricted amorphization; ■, complete amorphization.

junction of three Zr_3Fe grains and irradiated at 250 keV. The three grains were identified by both compositional and diffraction analyses as being orthorhombic Zr_3Fe. One grain has turned completely amorphous, while the other grains show no signs of amorphization (as evidenced by diffraction analysis) or of any form of damage upon post-irradiation examination. In the data shown in Fig. 4, the experimental point for the irradiation at

250 keV was labelled "restrictive amorphization", because of the above behavior.

The dependence of amorphization on sample orientation can also be seen in Fig. 5(b) from an irradiation performed at 300 keV. Here, the amorphous spot does not exactly follow the shape of the beam but contains "wisps" of amorphous material (shown arrowed) in directions that follow the bend contours of the thin sample. Such an orientation dependence disappears above 400 keV. An orientation dependence of the dose-to-amorphization under electron irradiation has been observed by Mori *et al.* in Zr_3Al [30] though at higher electron energies. This orientation dependence can be qualitatively explained if the damage-producing process operates preferentially along particular lattice directions, *i.e.* if the displacement energy is orientation dependent.

The results of the energy dependence experiments can be analysed in terms of a composite displacement cross-section dominated at high energies (700–900 keV) by displacements of Zr and Fe atoms; by displacement of Fe atoms at intermediate energies (400–600 keV); and by secondary displacements of lattice atoms by recoil impurities at low energies (below 400 keV). One of the most predominant recoil impurities will be oxygen. Preliminary measurements using an elastic recoil detection technique indicate oxygen levels of 1–3 at.% in the bulk of the Zr_3Fe alloy, so a value of 1 at.% was used in the analysis discussed below. If the same amorphization mechanism is operative at all electron energies, then
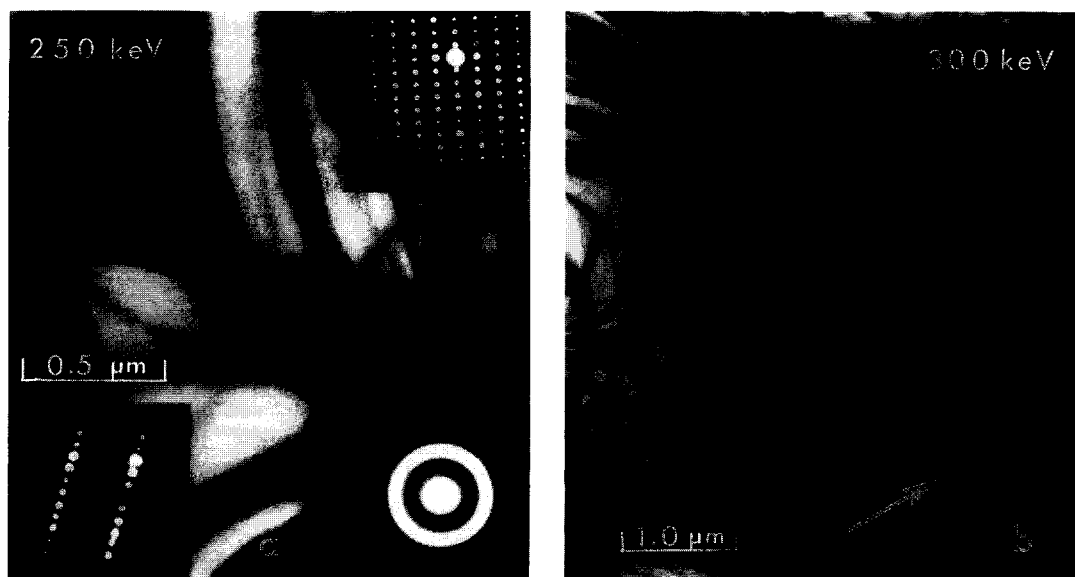

Fig. 5. (a) Bright-field electron micrographs and associated diffraction patterns, showing the strong orientation dependence of the damage production for Zr_3Fe irradiated with 250 keV electrons at 23–30 K. The irradiation was performed at a triple junction and only one of the Zr_3Fe grains at this junction has been rendered amorphous by the irradiation. The electron fluence was 6.8×10^{22} e$^-$ cm^{-2}. (b) Bright-field electron micrograph, showing indications of orientation dependence of damage production for Zr_3Fe irradiated at 23–30 K with 300 keV electrons to a fluence of 5.2×10^{22} e$^-$ cm^{-2}.

the total dose D (in displacements per atom (dpa)) required to produce amorphization in Zr_3Fe (considering both primary and secondary displacement mechanisms) should be independent of the electron energy. The displacement energies of the Zr and Fe atoms were adjusted to give the smallest variation in D from 250 to 950 keV. The set that gave the best results was $E_d^{Zr} = 24$ eV and $E_d^{Fe} = 14$ eV.

In this analysis, which should be considered as being preliminary, the orientation dependence of the displacement and scattering cross-sections was neglected; oxygen was considered as the major impurity; secondary displacements in the Fe sublattice of Zr_3Fe were considered, but those in the Zr sublattice were neglected; and the displacement cross-sections used were those given by Owen [31]. A more detailed discussion of the energy dependence results will be given elsewhere [32]. The displacement per atom values given in Fig. 3 were obtained using a value of $E_d = 25$ eV for Zr_3Fe for the conversion from electron and ion fluences to displacements per atom.

3.3. Irradiation-induced amorphization of $ZrFe_2$, $ZrCr_2$, $Zr(Cr,Fe)_2$ and $Zr_2(Ni,Fe)$

Investigations have been initiated on various Zr–Fe–Cr intermetallic compounds to obtain information on the details of the damage structure in individual cascades, the critical temperature for amorphization by ions and electrons, and the effects of lattice defects, such as dislocations and stacking faults, and variation in stoichiometry on the dose required to produce amorphization. For example, the critical temperatures for the amorphization of $ZrCr_2$, $Zr(Cr,Fe)_2$ and $ZrFe_2$ by irradiation with electrons of energy 0.9 MeV was found to be 150–200 K, about 225 K and about 100 K respectively. Since all these compounds have the same Laves phase structure, the stoichiometry of the compound may play an important role. Also, in $ZrFe_2$, small grains that are heavily faulted amorphize more readily than do larger grains that contain relatively few stacking faults. There is prior evidence from studies on other intermetallic compounds that preferential amorphization can occur at grain boundaries [33], dislocations [34], free surfaces [35] and antiphase boundaries [36]. These are high-energy regions and the local distortion of the lattice or high chemical energy gives an additional contribution to the free energy rise resulting from irradiation, thus enhancing the crystalline-to-amorphous transformation.

Studies were performed on thin foils of zircaloy-4 irradiated at 300–650 K with ^{40}Ar ions of energy 350 keV in the dual-ion-beam HVEM facility at ANL. The irradiation-induced amorphization of the intermetallic precipitates $Zr(Cr,Fe)_2$ and $Zr_2(Ni,Fe)$ was studied *in situ*. Details of this investigation are given elsewhere [13]. Here, the results will be discussed in the context of previous experimental results of neutron and electron irradiations.

The basic features of irradiation-induced amorphization of $Zr(Cr,Fe)_2$ and $Zr_2(Ni,Fe)$ precipitates in Zircaloy-4 may be summarized as follows.

(1) Under electron irradiation, both types of precipitate amorphize if the irradiation temperature is lower than 300 K. Amorphization happens homogeneously and is thought to occur as a result of increased chemical disordering and a higher concentration of the less mobile point defect caused by the loss of the more mobile defect to the free surface [37].

(2) Under low-temperature neutron irradiation, amorphization occurs for both types of precipitate, through some combination of cascade chemical disordering and bulk point defect concentration increase. Under high temperature neutron irradiation, the $Zr_2(Ni,Fe)$ precipitates remain crystalline and the $Zr(Cr,Fe)_2$ precipitates amorphize, while developing a duplex structure, with amorphization starting at the precipitate–matrix interface and proceeding inwards [1–4]. It has been proposed [38] that in the case of $Zr(Cr,Fe)_2$ precipitates, amorphization occurs by a combination of less effective cascade disordering and a departure from exact stoichiometry at the precipitate–matrix interface caused by ballistic mixing.

(3) Under ^{40}Ar ion irradiation [13], the $Zr(Cr,Fe)_2$ precipitates amorphize at temperatures up to 650 K, while the $Zr(Ni,Fe)_2$ precipitates do so at least up to 600 K. Amorphization occurs homogeneously and without any associated changes in chemical composition. The amorphization mechanism is thought to be chemical disordering and possibly defect clustering induced by collision cascades. There is no need for a supplement from other mechanisms, such as a departure from stoichiometry, because, as a result of its higher damage rate, the damage produced by ion irradiation is more effective than that produced by neutron irradiation in causing amorphization.

4. Conclusions

Ion and electron irradiations have been used to obtain information on irradiation-induced crystalline-to-amorphous transformations in Zr intermetallic compounds. In Zr_3Fe, investigations of the role of the deposited-energy density $\bar{\theta}_v$ in the collision cascade revealed that, with decreasing $\bar{\theta}_v$, there was an increasing tendency for multiple damaged regions (subcascades) to form within a main cascade, and the fraction of the theoretical collision cascade volume that was occupied by the visible damaged regions decreased rapidly. The critical temperature for the amorphization of Zr_3Fe by electron irradiation was about 220 K, compared with

570–600 K for ^{40}Ar ion irradiation, and this difference was attributed to the fact that ion irradiation produces displacement cascades, while electron irradiation produces isolated Frenkel pairs.

The dependence of the damage production (dose-to-amorphization) on the incident electron energy was determined for Zr_3Fe and the results could be analysed in terms of a composite displacement cross-section dominated at high energies (700–900 keV) by displacements of Zr and Fe atoms; by displacements of Fe atoms at intermediate energies (400–600 keV); and by secondary displacements of lattice atoms by recoil impurities at low energies (below 400 keV). At low electron energies (250–350 keV), the dose-to-amorphization (in electrons per square centimeter) of Zr_3Fe was dependent on the orientation of the sample relative to the electron beam. Studies on $ZrFe_2$, $Zr(Cr,Fe)_2$ and $ZrCr_2$ indicated that variations in the stoichiometry and the presence of lattice defects may have an appreciable effect on the irradiation-induced amorphization process. Mechanisms were also proposed for the amorphization of $Zr(Cr,Fe)_2$ and $Zr_2(Ni,Fe)$ precipitates in Zircaloy-4 during electron, ion and neutron irradiation.

Acknowledgments

References

1 W. J. S. Yang, R. P. Tucker, B. Cheng and R. B. Adamson, J. Nucl. Mater., 138 (1986) 185.

2 M. Griffiths, J. Nucl. Mater., 159 (1988) 190.

3 F. Lefebvre and C. Lemaignan, J. Nucl. Mater., 165 (1989) 122.

4 A. T. Motta, F. Lefebvre and C. Lemaignan, in C. M. Euken and A. M. Garde (eds.), Proc. 9th Int. Symp. on Zirconium in the Nuclear Industry, ASTM Spec. Tech. Publ., 1132 (1991) 718.

5 L. M. Howe, D. P. McCooeye, M. H. Rainville, J. D. Bonnett and D. Phillips, Nucl. Instrum. Methods B, 59–60 (1991) 884.

6 L. M. Howe, M. H. Rainville and D. Phillips, in G. S. Was, L. E. Rehn and D. M. Follstaedt (eds.), Phase Formation and Modification by Beam–Solid Interactions, Mater. Res. Soc. Symp. Proc., 235 (1992) 461.

7 L. M. Howe, M. H. Rainville, D. Phillips, H. Plattner and J. D. Bonnett, Nucl. Instrum. Methods B, 80–81 (1993) 79.

8 A. T. Motta, L. M. Howe and P. R. Okamoto, J. Nucl. Mater., 205 (1993) 258.

9 H. Mori, H. Fujita, M. Tenda and M. Fujita, Scr. Metall., 18 (1984) 783.

10 G.-B. Xu, M. Meshii, P. R. Okamoto and L. E. Rehn, J. Alloys Comp., 194 (1993) 401.

11 M. Griffiths, R. W. Gilbert and V. Fidleris, in L. F. P. Van Swam and C. M. Euken (eds.), Proc. 8th Int. Symp. on Zirconium in the Nuclear Industry, ASTM Spec. Tech. Publ., 1029 (1989) 658.

12 M. Griffiths, Philos. Mag. A, 68 (1991) 835.

13 A. T. Motta, L. M. Howe and P. R. Okamoto, in M. Nastasi, L. R. Harriott, N. Herbots and R. S. Averback (eds.), Beam–Solid Interactions: Fundamentals and Applications, Mater. Res. Soc. Symp. Proc., 279 (1993) 517.

14 R. S. Walker and D. A. Thompson, Radiat. Effects, 37 (1978) 113.

15 L. M. Howe, M. H. Rainville, H. K. Haugen and D. A. Thompson, Nucl. Instrum. Methods, 170 (1980) 419.

16 L. M. Howe and M. H. Rainville, Nucl. Instrum. Methods, 182–183 (1981) 143.

17 L. M. Howe and M. H. Rainville, Nucl. Instrum. Methods B, 19–20 (1987) 61.

18 L. M. Howe and M. H. Rainville, in U. Gibson, A. E. White and P. P. Pronko (eds.), Materials Modification and Growth Using Ion Beams, Mater. Res. Soc. Symp. Proc., 93 (1987) 79.

19 K. B. Winterbon, P. Sigmund and J. B. Sanders, K. Dan Vidensk. Selsk. Mat. Fys., Medd., 37 (1970) 14.

20 K. B. Winterbon, Ion Implantation Range and Energy Deposition Distributions, Vol. 2, Plenum, New York, 1975.

21 M. O. Ruault, J. Chaumont and H. Bernas, IEEE Trans. Nucl. Sci., 30 (1983) 1746.

22 M. O. Ruault, J. Chaumont and H. Bernas, Nucl. Instrum. Methods, 209–210 (1983) 351.

23 M. O. Ruault, J. Chaumont, J. M. Penisson and A. Bourret, Philos. Mag. A, 50 (1984) 667.

24 J. Narayan, D. Fathy, O. S. Oen and O. W. Holland, Mater. Lett., 2 (1984) 211.

25 J. R. Parsons and C. W. Hoelke, Radiation Effects in Semiconductors, Plenum, New York, 1968, p.339; IEEE Trans. Nucl. Sci., 16(6) (1969) 37.

26 M. G. Kalitzowa, D. J. Karpuzov and N. K. Pashov, Philos. Mag. A, 51 (1985) 373.

27 A. Carbone, L. McCurdy, C. Koch and D. I. Potter, Scr. Metall. Mater., 26 (1992) 1321.

28 L. M. Howe, A. T. Motta and P. R. Okamoto, unpublished results, 1992.

29 J. Koike, P. R. Okamoto, L. E. Rehn and M. Meshii, in L. E. Rehn, J. E. Greene and F. A. Smidt (eds.), Processing and Characterization of Materials Using Ion Beams, Mater. Res. Soc. Symp. Proc., 28 (1989) 339.

30 H. Mori, M. Nakamima and H. Fujita, Proc. 11th Int. Cong. on Electron Microscopy, Kyoto, 1986, p.1101.

31 O. S. Owen, ORNL Rep. 4897, 1973.

32 A. T. Motta, L. M. Howe and P. R. Okamoto, Proc. Symp. on Ion Beam Synthesis and Processing, 1993 Fall Meeting of the Materials Research Society, Boston, MA, 1993, in press.

33 D. E. Luzzi, H. Mori, H. Fujita and M. Meshii, Acta Metall., 34 (1986) 629.

34 H. Mori, H. Fujita and M. Fujita, Jpn. J. Appl. Phys., 22 (1983) L94.

35 H. Mori, H. Fujita and M. Fujita, Proc. 75th Int. Conf. on HVEM, Berkeley CA, 1983, p.223.

36 H. Mori and H. Fujita, in H. Suzuki (ed.), Proc. Yamada Conf. on Dislocations in Solids, University of Tokyo Press, Tokyo, 1985, p.563.

37 A. T. Motta and D. R. Olander, Acta Metall. Mater., 38 (1990) 2175.

38 A. T. Motta and C. Lemaignan, J. Nucl. Mater., 195 (1992) 277.